NDP Experiment Time Application

Neutron Physics Laboratory - Nuclear analytical methods with neutrons

Xin Yang

Proposal ID

158

The NaCl sample shows almost no measurable N content – to analyze the sample, higher neutron beam intensity (> 10^8 $cm^{-2}s^{-1}$) should be used. Another possible reason is that the NaCl film will dissolve into the moisture if long-term exposure to the air, which makes no Cl viewed in the sample.

The melamine sample was measured two times (D574, C575) with the similar results, i.e. homogenous N profile from the sample surface up to the depth of about 1 micron. The N concentrations are calculated as for stoichiometric melamine with density 1.57 $g.cm^{-3}$. The total N content calculated with respect to the N content in the Si_3N_4 standard (measured under the same conditions) is about 3.7 x 10^{19} N $at.cm^{-2}$.

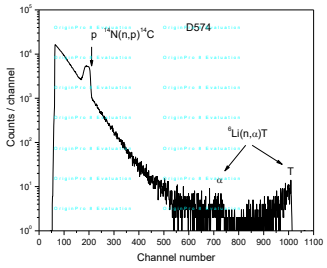

(a) The spectrum

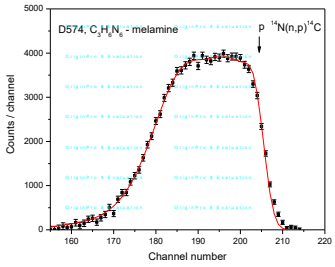

(b) Fitted spectrum of N

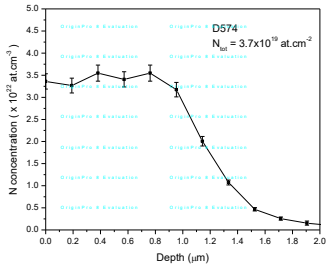

(c) N Profiling

Fig 1 Measurement D574

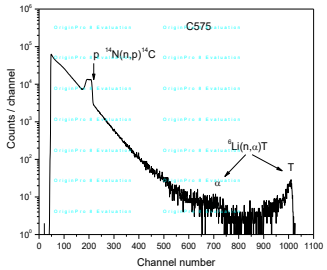

(a) The spectrum

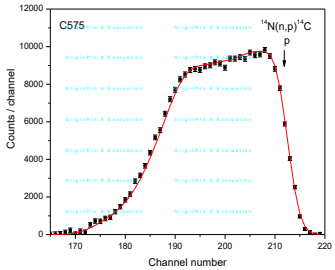

(b) Fitted spectrum of N

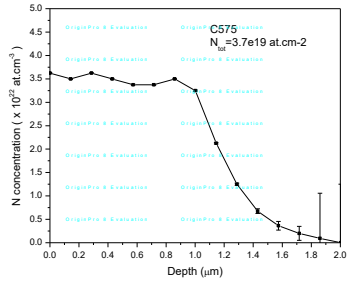

(c) N Profiling

Fig 2 Measurement C575

Effect of high LET radiation on specific interaction of proteins with DNA.

Laboratory of Cyclotron and Fast Neutron Generators

Marie Davidkova

Proposal ID

52

The project “Effect of high LET radiation on specific interaction of proteins with DNA” is a contribution of our laboratory to the international COST project MP1002 "Nano-scale insights in ion beam cancer therapy (Nano-IBCT)“. The laboratory is a member of working group WG5 Radiobiological effects (detection of DNA double strand breaks, prediction and cell damage). The goal of the project is to determine how radiation damage of repair proteins influences rate and fidelity of repair mechanisms in cells. Irradiation of biological samples at accelerators of the Nuclear Physics Institute ASCR in Řež (cyclotron U120M and tandetron) is specific by low energies of incident proton beam. Maximal proton energy at cyclotron U120M is approximately 34 MeV, at tandetron 6 MeV. The range of these ions in water is only several tens of micrometers (range of 6 MeV protons in water is approximately 0.5 mm, in case of 34 MeV protons about 11 mm). Therefore, the experiments should be performed with thin biological samples.

Several particular experimental setups has been designed and tested:
a) own developed prototype rings from plastic or metal extending thin Mylar foil
b) sterile Petriho dishes with glass bottom
c) commercially available plastic dishes with cover and bottom from Mylar foil (Chemplex, USA).
As the best solution for further experiments with neonatal dermal fibroblasts seems the last proposed setup using plastic dishes. Petri dishes with glass bottom will be used for experiments with our colleagues from Biophysical Institute ASCR, which analyze irradiated samples by FISH technique (fluorescence in situ hybridization). Cells are seeded 24 h before irradiation and grown directly on glass slide. DNA plasmids in water solution are irradiated in thin plastic tubes.

The proportion of direct and indirect effects in proton tracks has been followed in pBR322 DNA plasmids in water solution. Samples were irradiated in presence of increasing concentrations of OH radical scavengers (coumarin-3-carboxylic acid, dimethylsulfoxid or glycylglycine). The yields of single and double DNA strand breaks were determined by agarose gel electrophoresis. The contributions of direct and indirect DNA damage in dependence on scavenger concentration has been determined for 30 MeV protons. The experiments will be extended for larger interval of proton energies and also other types of ions.

Radiation damage to proteins has been studied for selected restriction enzymes HindIII and PvuII. Enzymes irradiated by increasing doses were subsequently with DNA pCDNA3 plasmids. Restriction enzymes recognize and cleave specific DNA base sequences. The functionality of irradiated restriction enzymes can be thus followed by agarose gel electrophoresis, where DNA fragments of known size can be easily visualized. Decrease of enzyme activity with increasing absorbed dose has been detected.

During the first year of the project, the results for cell cultures have not been planned. In the frame of planning of experimental studies, methods and experimental setup has been proposed and prepared. The first pilot experiments have been realized too. Cell survival curves have been determined for confluent neonatal fibroblasts grown on 2.5 μm Mylar foils and irradiated by gamma radiation and 15 and 30 MeV protons. In irradiated samples the cell survival and micronuclei formation has been determined. Experiments will be repeated, extended and analyzed. In collaboration with Biophysics Institute ASCR, the first experiments focused to DSB repair in normal neonatal skin fibroblasts have been performed.

Elemental characterization of Neolithic and Byzantine archeological samples using k0-NAA

Neutron Physics Laboratory - Nuclear analytical methods with neutrons

Sema Erenturk

Proposal ID

155

Elemental characterization of Neolithic and Byzantine archeological samples using k0-NAA

The purpose of this study is to investigate the elemental concentrations of archeological ceramics which were found in Yenikapı (İstanbul) during the construction of underground metro to get information on provenance of the findings, technologies, material culture and the organization of artefact production.

Ceramic findings were milled with IKA Mill for 1-2 min. After these procedures the samples were sent to Nuclear Physics Institute AS CR in Řež, Czech Republic. Here, the samples were milled again in the agate mortar for 5 min. to ensure the homogeneity. Major elements (namely Si, Al, Ca, Mg, Na, Fe, Ba) and minor elements (namely As, Br, Cd, Cr, Cu, Fe, Mn, Ni, Sb, Sr, Ti, Th, U, Zn) in the samples were determined by neutron activation analysis (NAA).

Short irradiation (1 min.) of the samples, Si standards and Au+Mn+Rb monitor sets was carried out in channel H1 of the LVR-15 reactor equipped with fast pneumatic transfer system. Gamma-ray spectra of samples and monitors were measured using a coaxial HPGe detector (PGT, relative efficiency 20.3 %, resolution FWHM 1.75 keV @1332.5 keV, peak-to-Compton (P/C) ratio 49.8:1).

For long-time irradiation, the samples, Ni standard and Au+Mo+Rb monitor sets were formed into a columns and hermetically sealed in three Al irradiation containers. The Al containers were irradiated in the LVR-15 reactor in channel H8 located at the outer perimeter of the LVR-15 reactor active core, in a Be reflector block, with the whole reactor spectrum for 3 hours. Gamma-ray spectra of samples and monitors were measured using a coaxial HPGe detector (Canberra, relative efficiency 77.8 %, resolution FWHM 1.87 keV @1332.5 keV, and peak-to Compton ratio of 82.5:1).

Two counts were performed for each sample after decay times of 5 days (time of measurement 90 min., measurement geometry 15 cm for ceramic, SRMs NIST 1633B, and 2711, and 1 cm for blank and SRM NIST 1547) and 6 weeks (time of measurement 6 hours, measurement geometry 1 cm for all samples). Measurement of the Au+Mo+Rb monitor sets was carried out in the geometry of 10 cm after a decay time of 4 days.

Results of k_0-NAA were calculated using the Kayzero for Windows program.

Acknowledgements

We are grateful to CANAM for providing technical support by the Nuclear Physics Institute AS CR in Řež, Czech Republic. We also thanks to Prof.Dr.Jan Kucera and Dr.Marie Kubesova for their effort and support during the project.

Effect of high LET radiation on specific interaction of proteins with DNA.

Laboratory of Cyclotron and Fast Neutron Generators

Marie Davidkova

Proposal ID

21

Průběžná zpráva o realizaci projektu za rok 2012

Projekt je řešen jako příspěvek řešitelského týmu k mezinárodnímu projektu COST MP1002 "Nano-scale insights in ion beam cancer therapy (Nano-IBCT, Nano-aspekty iontové terapie nádorů)“. Řešitelská laboratoř je součástí pracovní skupiny WG5 Radiobiologické efekty (detekce dvojných zlomů DNA, predikce a buněčné projevy poškození). Cílem projektu je určit jakým způsobem ovlivňuje radiační poškození reparačních proteinů rychlost a správnost reparačních mechanismů v buňkách.

Ozařování biologických vzorků na urychlovačích v ÚJF v Řeži, cyklotron U120M a tandetron, je specifické díky energiím dostupných nabitých částic. Maximální energie protonů na cyklotronu U120M je přibližně 34 MeV, na tandetronu 6 MeV. Dosah těchto iontů ve vodě je pouze několik desítek μm až mm (protony 6 MeV mají ve vodě dosah přibližně 0,5 mm, 34 MeV 11 mm), proto je třeba pracovat s tenkými vrstvičkami vzorků.

Bylo navrženo a testováno několik možných řešení:

a) Prototypové plastové nebo kovové kroužky držící velmi tenkou Mylar folii vyrobené v ODZ ÚJF
b) Sterilní Petriho misky s kruhovým otvorem ve dně, na které je nalepeno krycí mikroskopické sklíčko
c) Komerčně dostupné plastové misky, u kterých je dno a případně i víčko nahrazeno Mylar folií (firma Chemplex, USA).

Navržená řešení byly testovány během ozařování na cyklotronu U120M. Pro další experimenty s neonatálními dermálními fibroblasty se jeví jako nejvhodnější řešení varianta c. Pro experimenty realizované ve spolupráci s kolegy z Biofyzikálního ústavu AV ČR v Brně, kdy byly buňky analyzovány metodou FISH (fluorescenční in situ hybridizace) se jeví výhodnější uspořádání v Petriho miskách (varianta b). Buňky rostou přímo na mikroskopickém sklíčku, po ozáření jsou dále zpracovány a analyzovány fluorescenčním mikroskopem. DNA ve vodných roztocích jsou ozařovány v úzkých plastových mikrozkumavkách.

Podíl přímého a nepřímého účinku ve stopách protonů byl studován s použitím DNA plasmidů pBR322 ve vodných roztocích. Vzorky obsahovaly různé koncentrace sloučenin vychytávající hydroxylové radikály (kumarin-3-karboxylová kyselina, dimethylsulfoxid nebo glycylglycin). Metodou agarózové elektroforézy byly stanoveny výtěžky jednoduchých a dvojných zlomů DNA. V závislosti na koncentraci vychytávače lze odhadnout podíl přímého poškození DNA a příspěvek nepřímého poškození prostřednictvím OH radikálů. Tyto informace budou velmi zajímavým výstupem projektu, zvláště pokud získáme větší rozsah různých iontů a energií.

Radiační poškození proteinů bylo studováno u restrikčních enzymů HindIII a PvuII. Enzymy ozářené rostoucími dávkami záření byly inkubovány s pCDNA3 plasmidy a vzorky byly poté analyzovány metodou agarózové elektroforézy. Funkční enzymy rozpoznávají specifickou sekvenci bazí a v tomto místě DNA štěpí. Proteiny poškozené zářením postupně ztrácejí schopnost rozpoznat a štěpit DNA. Bylo sledováno snižování aktivity enzymů s rostoucí dávkou záření.

V prvním roce řešení projektu nebylo plánováno získání výsledků pro buněčné kultury. V rámci přípravy byly nicméně připraveny metodiky pro realizaci experimentů, potřebné laboratorní uspořádání a byly realizovány první pilotní experimenty. Křivky přežití byly měřeny pro konfluentní neonatální fibroblasty pěstované na 2,5 μm Mylar foliích a ozářených rostoucími dávkami gama záření a 15 a 30MeV protonů. V ozářených vzorcích bylo stanoveno přežití buněk a četnost výskytu mikrojader. Experimenty budou zopakovány, doplněny a analyzovány. Ve spolupráci s Biofyzikálním ústavem AV ČR, v.v.i. proběhly i první experimenty zaměřené na reparaci DSB v neonatálních fibroblastech v závislosti na struktuře chromatinu v buněčném jádru.

Effect of applied magnetic field on internal structure of multiferroi nanocomposites

Neutron Physics Laboratory - Neutron diffraction

Aleksandr Naberezhnov

Proposal ID

228

Effect of applied magnetic field on internal structure of nanocomposites with coexisting magnetic and ferroelectric orderings

Instrument MAUD. Experimental team V. Ryukhtin, A. Naberezhnov

The principle idea of measurements was to study of temperature evolution of internal organization of ferroelectric nanoparticles embedded into magnetic porous glasses near the ferroelectric phase transition at application of external magnetic fields.

We have used two types of nanocomposites (NCM) on base of microporous magnetic glasses Fe4-MIP with average pore diameter ~ 5 nm. The first type contained the sodium nitrite (NaNO2) where we have earlier observed the crossover [1] of the ferroelectric phase transition from the first order to the second one. The second nanocomposite contained the potassium nitrate (KNO3). In KNO3 the ferroelectric phase exists in the temperature interval 397 – 378 K at cooling only, but in a restricted geometry this phase becomes stable at cooling down to 100 K [2]. NaNO2 and KNO3 were introduced into the pores from the melt. In Figure the results of SANS data at 310 K (a) and 438 K (b) for NCM NaNO2+Fe4-MIP are presented.

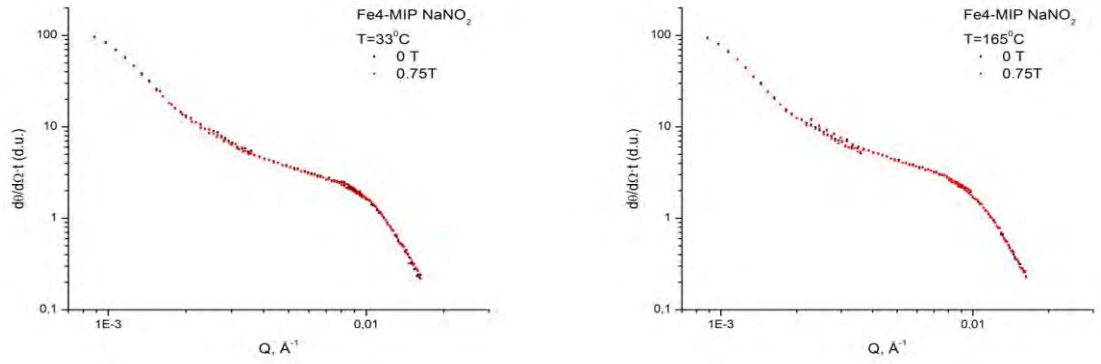

(a) (b)

Figure *S(Q) for Fe4-MIP with NaNO2 embedded into the pores. Black points correspond to zero field, red points - at field 0.75 T.*

The anomalies at small Q and at Q~0.01 $Å^{-1}$ correspond to magnetic nanoparticles which we have earlier observed in our studies of empty microporous magnetic glasses. It is easy to see that there is no effect of applied magnetic field (up to B=0.75 T) on their space organization. It confirms our results devoted to study of magnetostriction in these glasses [3] where it have been shown that the magnetostriction has appeared at B above 1 T. Unfortunately we had no possibility to apply the field higher 1 T due to experimental restrictions. The scattering objects at Q~ 2×10^{-3} $Å^{-1}$ correspond to the embedded ferroelectrics and demonstrate a weak dependence on temperature. The dependence on applied magnetic field for ferroelectric nanoparticles we could not observed due to insufficient magnetic field.

References

1 A. Naberezhnov, A. Fokin, Yu. Kumzerov , A. Sotnikov , S. Vakhrushev, and B. Dorner, "Structure and properties of confined sodium nitrite", ***Eur. Phys. J.*** **E 12**, s21-s24 (2003)

2 A. Naberezhnov, E. Koroleva, E. Rysiakiewicz-Pasek, A. Fokin, A. Sysoeva, A. Franz, M. Seregin and M. Tovar "Phase transitions in nanostructured potassium nitrate" ***Phase Transitions*** , 87, 1148-1156 (2014)

3 A. Naberezhnov, N. Porechnaya, V. Nizhankovskii, A. Filimonov, and B. Nacke "Morphology and Magnetic Properties of Ferriferous Two-Phase Sodium Borosilicate Glasses" ***The Scientific World Journal***, Volume 2014, Article ID 320451, 7 pages, (2014)

Influence of interlamellar spacing on the phase stresses in cold rolled pearlitic steel.

Neutron Physics Laboratory - Neutron diffraction

Jeroen Tacq

Proposal ID

78

Influence of interlamellar spacing on the phase stresses in cold rolled pearlitic steel

The cold rolled steel sheets on which residual strain measurements were to be performed, were bend as an inevitable consequence of cold rolling. As a result, it proved impossible to reliably measure the residual strains. An alternative experiment was therefore set up.

Instead of measuring residual strains, the internal strain evolution during in-situ tensile tests were measured. Specially designed clamps were used to fix the sample to the tensile rig. Four different types of samples were available: (1) Undeformed pearlite, with a microstructure consisting of randomly oriented lamellae. (2) Pearlite cold rolled to a strain of 1.1, with lamellae aligned to the rolling plane. (3) Same as second sample, but heat treated to remove the residual strains present after rolling. (4) Spheroidised pearlite, with a microstructure consisting of a fine dispersion of cementite particles. During the in-situ tensile test, the samples were also subjected to unloading-loading cycles. Four ferrite diffraction peaks were measured (200, 211, 220 and 310). Both the ferrite lattice strain and peak width were analysed.

Although a number of trials were required, very good, high quality results were eventually obtained, thanks to the patience and hard work of the instrument responsible. The main experimental results were the observations that (1) the intergranular strain development is very limited, (2) the internal strain evolution changes significantly with a changing cementite morphology and (3) the diffraction peak width increases with loading, but decreases again as a result of unloading.

The first result can be understood from the fact that the local material properties mainly depend on the local cementite morphology. It is therefore local changes in the morphology that cause strain differences between different regions, rather than the ferrite crystal orientation.

The second result led to the conclusion that load transfer from ferrite to cementite is less efficient in a spheroidised microstructure as compared to a lamellar microstructure. The evidence for this was the observation of an increasing ferrite lattice strain in the spheroidised sample as compared to an almost constant lattice strain in the undeformed, lamellar pearlite. The cold rolled pearlite exhibits a decreasing ferrite lattice strain with increasing tensile strain. The is attributed to an even more efficient load transfer to the harder cementite phase, made possible by the lamellae alignment. This decreasing lattice strain can however not be explained if, as is often assumed, the ferrite and cementite lamellae undergo the same total strain. In the real material, both phases must therefore deform by a different amount, even within the confines of a lamellar microstructure.

The third result cannot be explained purely by a decreasing dislocation content or a reorganisation of the dislocations present, because the drop in peak width is too large. It is therefore proposed that significant strain gradients exist within pearlite, on length scales ranging from the interlamellar spacing to the colony size. The elastic component of these strain gradients can relax during unloading, leading to the observed decreasing diffraction peak width. The plastic component of the strain gradients can introduce additional dislocations in pearlite, contributing to the large strengths achieved by heavily deformed pearlite.

In summary, it can be said that two new, interesting aspects of the deformation of pearlite were revealed. In a real pearlite the iso-strain assumption doesn't hold and the ferrite and cementite phases can deform by a different amount. Because compatibility has to be maintained at the ferrite-cementite interfaces, this leads to the introduction of strain gradients on the scale of the lamellae. Additional inhomogeneity of the microstructure could also lead to strain gradients on a larger length scale. A publication is underway to report these findings to the scientific community.

Cross section measurements of deuteron induced reactions

Laboratory of Cyclotron and Fast Neutron Generators

Eva Šimeková

Proposal ID

48

The proton and deuteron induced reactions are of a great interest for the assessment of induced radioactivity of accelerator components, targets and beam stoppers. Continuing our previous deuteron activation measurements on Al, Cu, Fe and Co, we measured excitation functions of reactions on Mn, Cr, W and Zr provoked by deuterons up to 20 MeV in three irradiations.

6.2.2013
We realized two runs. In the first one a Cr foil (together with Al foils serving for beam energy attenuation and as an additional monitor) was irradiated by deuteron with initial energy 19.76 MeV during 5 min with a mean current 0.15 μA. The stacked–foil activation technique was utilized to irradiate Mn foils (initial deuteron beam energy 19.76 MeV, irradiation time 5 min, mean current 0.32 μA) in the second run. The excitation function for 55Mn(d,p)56Mn 55Mn(d,2np+)54Mn and 55Mn(d,4np+)52Mn were provided for the deuteron energy range 2-20 MeV.

28.8.2013
Two runs were realized. It was performed a run (initial deuteron energy 20.09 MeV, similar condition as 6.2.2013) to irradiate single Cr foil and a stacked-foil activation technique was utilized to irradiate W foils in the second run. The foil activities measured by two HPGe detectors are processed now.

9.10.2013
Two runs were realized. It was performed a run (initial deuteron energy 20.025 MeV, similar condition as 6.2.2013) to irradiate single Cr foil and a stacked-foil activation technique was utilized to irradiate Zr foils in the second run. The activity measurements are proceeded to obtain values for long living isotopes.

We obtained cross section values for for 48V, 49Cr 52mMn, 52Mn, 54Mn generated by deuteron induced reactions on Cr.

Determination of concentration of boron atoms on Ag surface by PGAA

Neutron Physics Laboratory - Nuclear analytical methods with neutrons

Tomáš Baše

Proposal ID

145

Ag films exposed to a methanol solution of isomer 9,12-$(HS)_2$-1,2-$C_2B_{10}H_{10}$ were analyzed using PGAA (Prompt Gamma-ray Activation Analysis) method to determine the concentration of boron. The concentration of nine samples with various exposure time were determined by PGAA. The absolute boron contents in these samples were converted into boron area density as the number of B atoms/cm^2. These results allow us to control the formation of Self-Assembled-Monolayers (SAM) on polycrystalline Ag films with respect to exposure time. They will be used in further development of metal-based materials with tunable physical and chemical properties.

Crystallographic and magnetic structure of BaxSr3-xCo2Fe24O41 hexagonal ferrites

Neutron Physics Laboratory - Neutron diffraction

Josef Buršík

Proposal ID

205

Crystal and magnetic structure of $Sr_{3-x}Ba_xCo_2Fe_{24}O_{41}$ hexagonal ferrites.

J. Buršík
Institute of Inorganic Chemistry ASCR, 250 68 Řež near Prague, Czech Republic.

Magnetoelectric (ME) multiferroics (*i.e.* materials combining coupled electric and magnetic dipoles have attracted great deal of research interest in the past years. Hexagonal ferrites of Z-type with general formula $Sr_{3-x}Ba_xCo_2Fe_{24}O_{41}$ have been recently found to show ME effects at room temperature and low external magnetic fields (0.01 T). They belong to a new family of ME multiferroics called magnetically induced ferroelectrics, where the ferroelectricity originated from a complex internal arrangements of magnetic moments. The substitution of small Sr for large Ba causes the change in the Fe(4)-O(2)-Fe(5) bond angle near the boundary of L and S blocks, which is a key component to induce noncollinear screw magnetic structures in these hexaferrites). The large Fe(4)-O(2)-Fe(5) bond angle in $Sr_{3-x}Ba_xCo_2Fe_{24}O_{41}$ may enhance the magnetic frustration at the boundary and thus stabilizes the spiral magnetic order. Therefore, the investigation of crystal and magnetic structure is of great interest for the study of multiferroic behavior in this system.

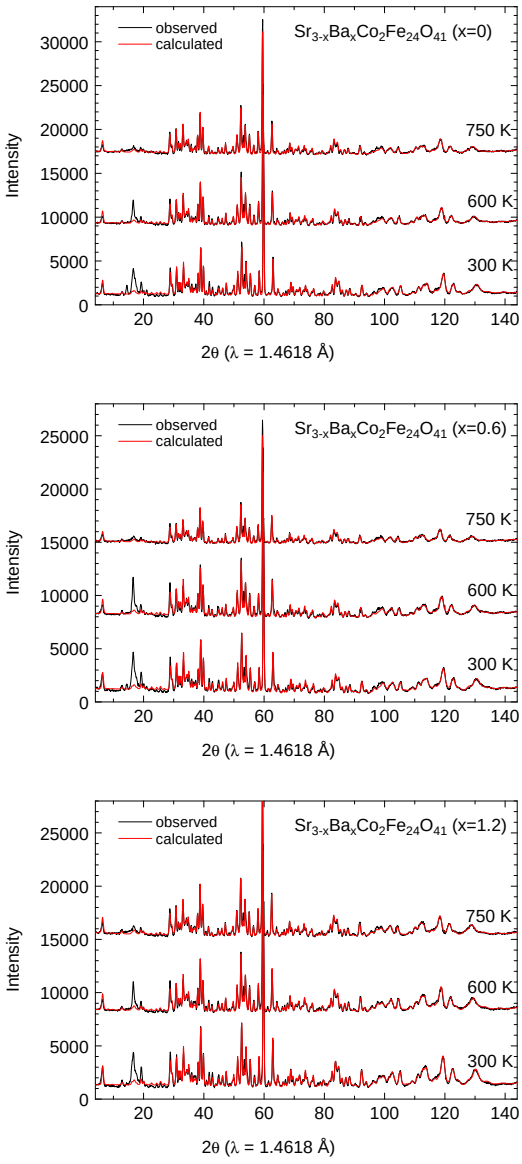

FIG. 1: Neutron diffraction patterns of $Sr_{3-x}Ba_xCo_2Fe_{24}O_{41}$ measured at temperatures 300, 600 and 750 K. Top: $x = 0$, middle: $x = 0.6$, bottom: $x = 1.2$.

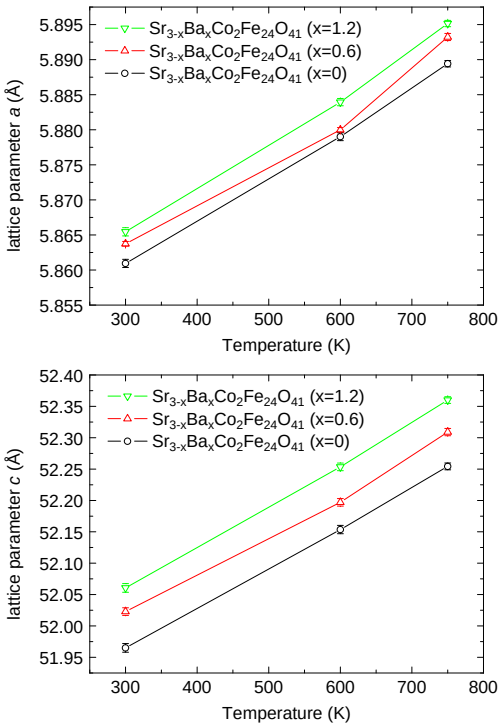

FIG. 2: Lattice parameters a (top) and c (bottom) dependence on temperature.

The acquired neutron diffraction patterns together with calculated profiles based on the crystal structure of $Sr_{3-x}Ba_xCo_2Fe_{24}O_{41}$ with $x = 0$, 0.6 and 1.2 for room temperature and 600 and 750 K are displayed in Fig. 1. Formation of single phase samples is confirmed by the patterns measured at 750 K, where no magnetic order is present. The main magnetic peaks emerged around 5.1 and 4.4 Å at lower temperatures 600 K and 300 K. The refinement of the complex magnetic structure will be subject of further study.

The ratio of Ba substitution into two different Sr/Ba sites was fixed for neutron refinement, because the scattering lengths of Sr and Ba (7.02 and 5.07 fm, respectively) are quite similar, and it will be refined with the help of X-ray diffraction, where the contrast between Sr and Ba is bigger. The largest relative shift of z-coordinate with increasing temperature is observed for oxygen atoms O(2) and O(3) and for iron atom Fe(3), which are close to Sr(1)/Ba(1) site, probably due to smaller temperature dilatation of ionic Sr/Ba-O bonds compared to covalent Fe-O and Co-O bonds.

The dependence of lattice parameters is displayed in Fig. 2. The lattice parameters follow a expected trend, *i.e.* they are linearly increasing with Ba content and with temperature.

Localisation of the stresses in two phase anisotropic materials

Neutron Physics Laboratory - Neutron diffraction

Andrzej Baczmanski

Proposal ID

176

Localisation of the stresses in deformed hexagonal polycrystalline material.

The aim of this proposal is to determine evolution of lattice strains and stress tensor for different orientations of grains in one phase Mg alloy during tensile test. Crystallographic texture (fibre type) of the cold rolled sample is shown in Fig.1. The stresses for different grain orientations can be calculated from the lattice strains measured for different orientations the of scattering vector with respect to the sample (changing sample orientation in Eulerian cradle and selecting hkl reflections by 2θ scattering angle). It should be stated that the methodology of stress measurement allows us to determine full stress tensor for grains having specific orientations directly from experiment [1].

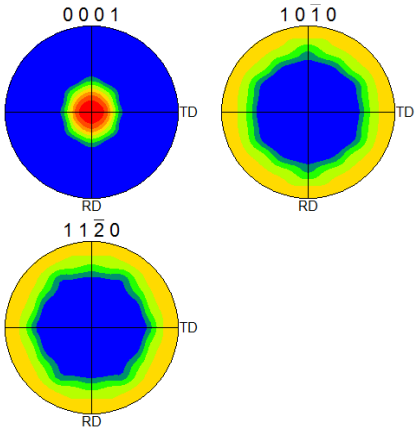

Fig.1. Pole figures for measured Mg sample.

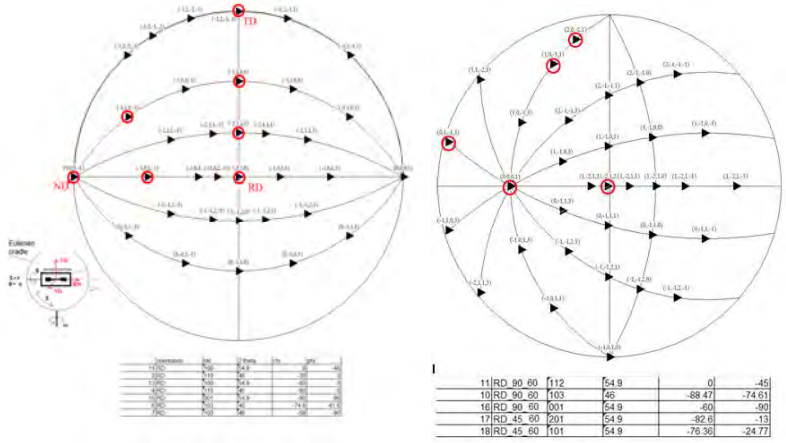

Fig. 2. Poles corresponding to two grain orientations for which the lattice strains were measured.

The interplanar spacings were measured with the wavelength of 1.196921Å (HK9 strain diffractometer) for the sample under different loads applied by small-rig, rotated in Eulerian cradle. The relative lattice strains were calculated with respect to the initial interplanar spacings (without applied load). To determine stress tensor for the preferred orientations, the lattice strains were measured independently for 22 orientations of the scattering vector (poles corresponding to two orientations of grains are shown in Fig. 2) with respect to the sample and for 15 different loads applied by a tensile rig (Fig. 3). Total time of measurements for one load (all poles) was about 20-22 hours.

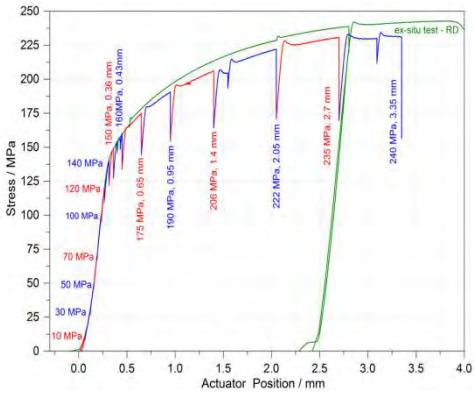

Fig. 3. Stress applied for the sample vs. actuator position. Loads for which the lattice strains were measured are indicated.

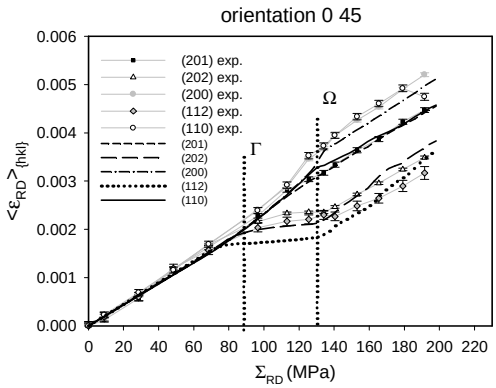

Fig. 4. Lattice strains measured along direction of applied load for different reflections (points) compared with model prediction.

Preliminary results of data analysis obtained for five different reflection and scattering vector parallel to the applied tensile load are shown in Fig. 4. The experimental lattice strains vs. applied load are compared with prediction of the selfconsistent model [2,3]. The best agreement between experimental and theoretical results was obtained for the critical resolved shear stresses (CRSS) given in Table 1. Therefore the values of CRSS for the main slip systems were established.

Slip system	< 11-20> (1-100)	< 1-210> (0001)	< 1-210> (10-10)	< 2-1-1-3> (10-11)
CRSS (MPa)	170	30	70	70

Tab. 1.

Data treatment is still in progress. We expect to observe significant difference between the stresses localised in the grains having different crystal orientations, especially during yielding. The determined stresses will be compared with prediction of the selfconsistent model. Also, a new experiment is planned to study the twinning phenomena and slips on crystallographic planes. In this experiment an acoustic emission will be recorded during elastoplastic deformation and the results will be compared with diffraction measurements.

REFERENCES:
[1] A. Baczmański, A. Gaj, L. Le Joncour, et al., ***Phil. Mag.***, 92 (2012) 3015-3035.
[2] A. Baczmański, C. Braham, ***Acta Mater.***, 59 (2004) 1133-1142
[3] P. Lipinski, M. Berveiller, E. Reubrez J. and Morreale, ***Arch. Appl. Mech.***, 65 (1995) 291.

The effect of carbon on interstitial ordering in epsilon-Fe3(C,N)1+x

Neutron Physics Laboratory - Neutron diffraction

Kenny Stahl

Proposal ID

178

CANAM experimental report – MEREDIT - 3.3.2015-5.3.2015

Kenny Ståhl & Bastian K. Brink

Neutron powder diffraction on ε-iron carbonitride

Scientific interest in the ε-iron nitride and carbonitride is founded by their metallurgical importance as they are formed on the surface of iron and steel hardened by nitriding and nitrocarburizing. The variation of long-range nitrogen ordering for ε-iron nitrides with various nitrogen contents has been studied as a function of both composition and temperature with neutron and X-ray diffraction [1,2,3]. Limited attention has however been paid to the carbonitrides but for a single sample a change in interstitial ordering compared to a nitride of similar total interstitial content has been observed [3].

The current experiment explored the effects of substitution of nitrogen by carbon on the interstitial ordering in $Fe_2(C,N)_{1-z}$. Superstructure reflections (001) and (301) were observed for two samples confirming the structural model in space group *P-31m* (compared to $P6_322$ for the pure nitrides). Refined occupancies indicated an increased degree of long-range order with only slightly increasing carbon content.

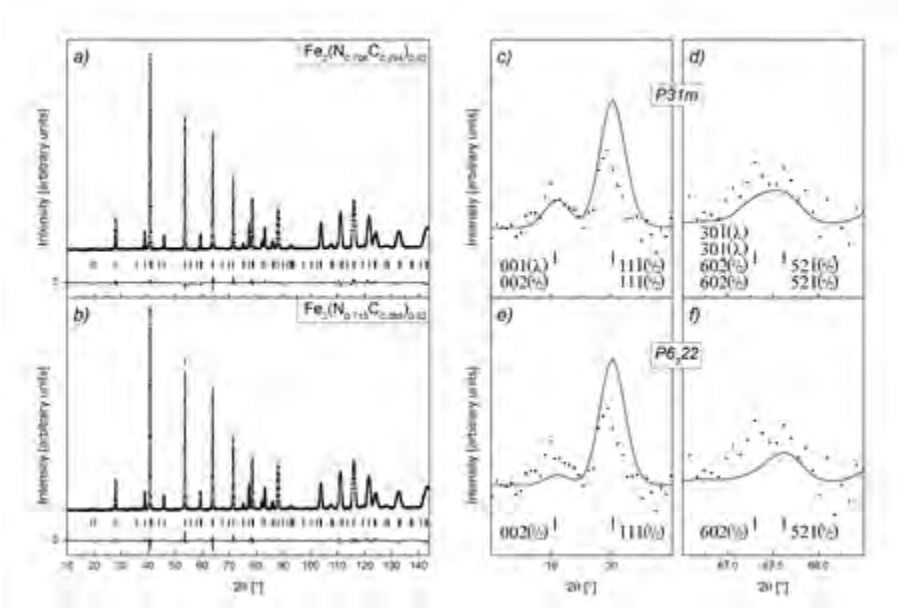

Figure 1: Neutron diffractogram (MEREDIT diffractometer, λ = 1.460 Å), refined Rietveld profile and difference curve for *a*) $Fe_2(N_{0.706}C_{0.294})_{0.92}$ and *b*) $Fe_2(N_{0.715}C_{0.285})_{0.92}$. Comparison of superstructure reflections of structural models in space group $P\bar{3}1m$ (*c+d*) and $P6_322$ (*e+f*) for $Fe_2(N_{0.715}C_{0.285})_{0.92}$. Note the $^{\lambda}/_{2}$-contribution (intensity ratio 0.004).

[1] A. Leineweber, H. Jacobs, F. Hüning, H. Lueken, H. Schilder, W. Kockelmann, J. Alloys Comp. 288 (1999) 79
[2] T. Liapina, A. Leineweber, E. J. Mittemeijer, W. Kockelmann, Acta Mater. 52 (2004) 173
[3] A. Leineweber, H. Jacobs, F. Hüning, W. Kockelmann, J. Alloys Comp. 316 (2001) 21

SANS studies of ferroelectrics embedded into magnetic porous glasses

Neutron Physics Laboratory - Neutron diffraction

Aleksandr Naberezhnov

Proposal ID

141

SANS studies of ferroelectrics embedded into magnetic porous glasses.

Instrument MAUD. Experimental team V. Ryukhtin, A. Naberezhnov

We have studied the inner structure of empty microporous (Fe20MIP) and macroporous (Fe20MAP) magnetic glasses and the composites on base of these matrices containing embedded ferroelectrics $NaNO_2$ and KNO_3. These composites are very interesting for creation of so-called artificial multiferroics with spatially separated ferroelectric and magnetic orderings [1-3]. In Figure the results of preliminary analysis of SANS data for the nanocomposites Fe20MIP+$NaNO_2$ and Fe20MIP+KNO_3 are presented. At treatment we have used the approximation of non-interactive spheres with log-normal distributions. The principle results for ferroelectric-containing samples are:

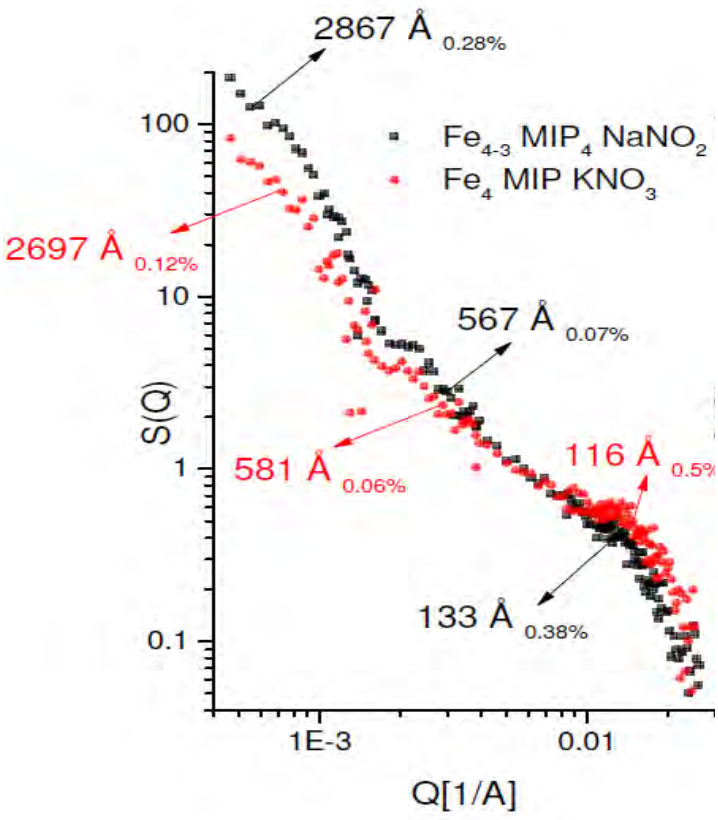

– There are three types of scattering objects with different characteristic sizes. The largest and the smallest objects correspond to the magnetic nanoparticles existing in these magnetic glasses and their sizes are in good agreement with AFM and X-rays diffraction data [4]. The middle size corresponds to the ferroelectric nanonoparticles and confirms the experimental observation that in porous glasses with small average pore diameters the embedded ferroelectrics form the dendrite network of independent clusters with the size essentially larger than average pore diameter (5 nm) in Fe20MIP glasses [5]. It is necessary to note that this results (in common with AFM, magnetic force microscopy, TEM and X-rays data [2-4]) is the first direct evidence of coexistence of two types magnetic particles and ferroelectric nanoclusters distributed in a volume of Fe20MIP and Fe20MAP glasses.

References

1 Manual Bibes, “Nanoferronics is a winning combination” ***Nature Materials*** 11, 354 – 357, (2012)

2 Alexander Naberezhnov et al, “Nanoporous Glasses with Magnetic Properties as a Base of High-frequency Multifunctional Device Making” ***Lecture Notes in Computer Science*** 8638, 459-466 (2014)

3 Alexander Naberezhnov et al., “Morphology and Magnetic Properties of Ferriferous Two-Phase Sodium Borosilicate Glasses” ***The Scientific World Journal***, Volume 2014, Article ID 320451, 7 pages, (2014)

4 T. V. Antropova, I. N. Anfimova, A. A. Naberezhnov et al.,“Structure of Magnetic Nanoclusters in Ferriferous Alkali Borosilicate Glasses” ***Physics of the Solid State***, 54(10), 2110–2115 (2012)

5 S. B. Vakhrushev, I. V. Golosovsky, A. A. Naberezhnov et al., “Structure and Dielectric Response of $Na_{1-x}K_xNO_2$ Nanocomposite Solid Solutions” ***Physics of the Solid State***, 50(8), 1548–1554 (2008)

Nanoscale investigation by SANS of case hardened steels for speed gears applications

Neutron Physics Laboratory - Neutron diffraction

Massimo Rogante

Proposal ID

210

CANAM_210 Report Form

The SANS measurements have been performed on all the scheduled Brugger specimens, namely A15 (17NiCrMo7 steel), C15 (9MnCr5 steel) and A45 (27MnCr5 steel).
Parts of these samples having the original thickness of 7 mm have been firstly investigated, with reference to a section of 15×1.5 mm^2. Two resolutions (medium and low) and a wavelength λ = 2.1Å have been adopted for these measurements.
Since the presence of a strong scattering effect, cut parts having a thickness of 1.1 mm have been also investigated, also with reference to a section of 15×1.5 mm^2.
Measurements were conducted in constant magnetic field in order to eliminate scattering of magnetic domains. Some of the obtained scattering curves are shown in Fig. 1.

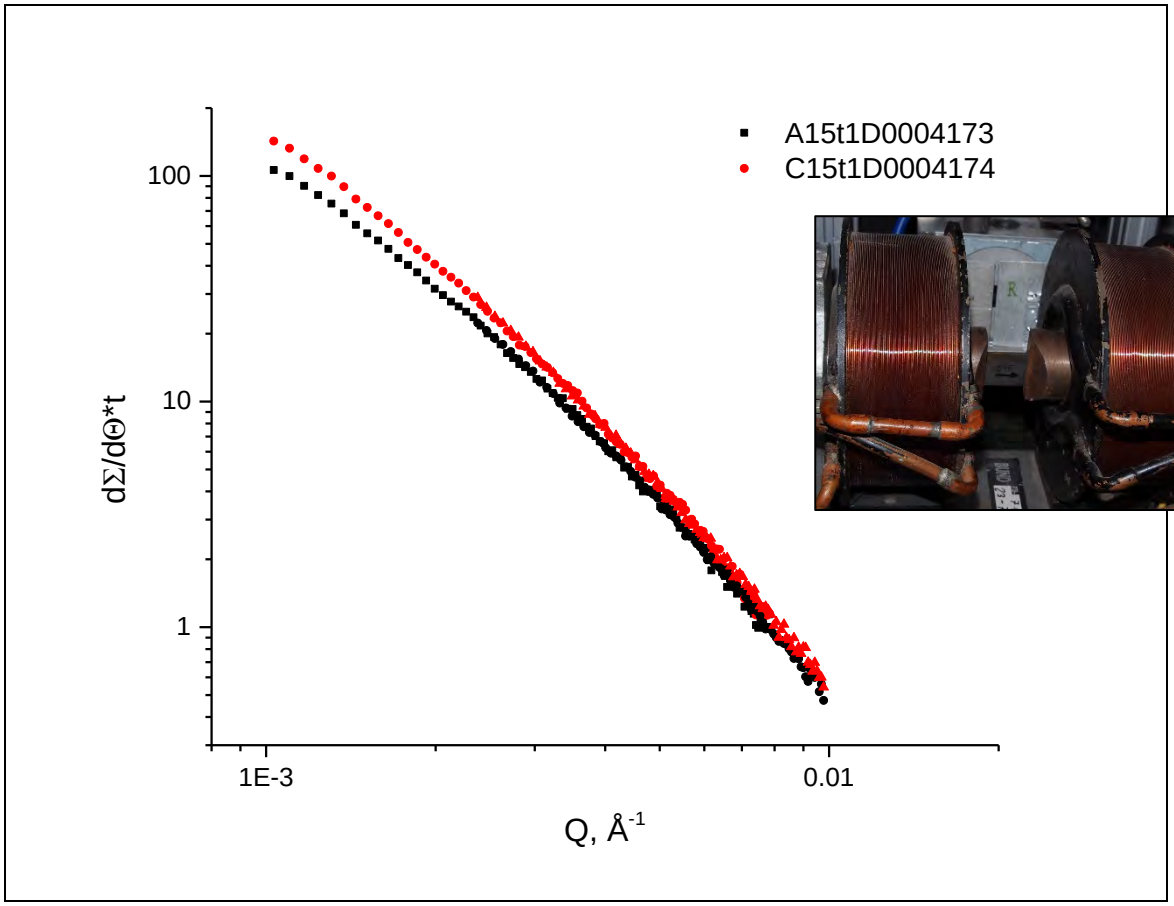

Fig. 1. SANS by samples A15 (black squares) and C15 (red circles) samples measured in DC magnetic field (1.2 T) **H**∥**Q** (see insert).

A sufficient difference results in scattering intensity between those samples. This is caused by different microstructure in these materials. Also usually micropores and cracks can substantially contribute to the scattering in this Q-range.
This SANS results would be used for microstructure characterization in combination with complimentary SEM/TEM analyses.
The definitive results of the present experiment are expected to be useful in the monitoring of the material's characteristics, giving a support in the life assessment of the related components.

Manganese iron borates

Neutron Physics Laboratory - Neutron diffraction

Christine Martin

Proposal ID

207

In the $Fe_{3-x}Mn_xBO_5$ solid solution, two compounds were studied: x = 1 and 1.5. In Fe_3BO_5, the 2 divalent and the 1 trivalent iron cations are not randomly distributed on the four crystallographic sites of the *Pbam* structure (shown below). Using two types of three legs ladders allows an easier description: one (Fe1 and Fe3 sites) is occupied by Fe^{+2} only and the other (Fe2 and Fe4 sites) by Fe^{+2} and Fe^{+3} (highlighted by white-I and yellow-II lines, respectively) [Phys. Rev. B79, 144408 (2009)]. The evolution of the cell parameters *vs.* x shows that manganese is introduced as divalent at the beginning of the series and NPD was necessary to confirm this x-dependence and more importantly to locate Mn and Fe on the cationic lattice.

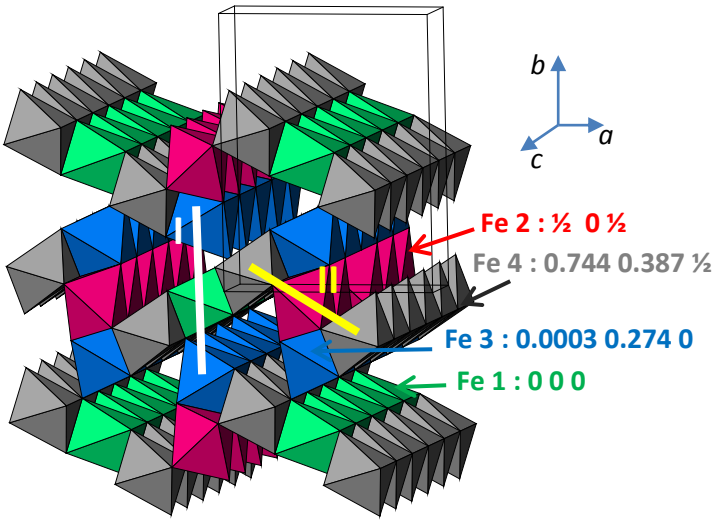

For x = 1, sites Fe1 and Fe3 are both occupied by Mn and Fe in a ratio close to 1, leading us to assume that the first (white) ladder contains divalent Mn and Fe cations. The trivalent Fe constitute thus the second one (yellow), the calculation giving a maximum of 3% of Mn on this ladder. For x = 1.5, the segregation is not so high: the ladders I and II are made of ≅ 74% and 26 of Mn, respectively. Moreover the distribution is different over both sites in each ladder: sites 1 and 2 are mainly occupied by Mn and Fe, respectively, whereas sites 3 and 4 are mixed with ≅ 73% and 26% of Mn. If the formula is, as expected, $Mn^{+2}_{1.5}Fe^{+2}_{0.5}Fe^{+3}_{1}BO_5$, it means that there is a redistribution of charges on the cationic lattice. A detailed analysis of the NPD data is currently in progress to confirm this point, to know if the description in two three legs ladders remains pertinent. Indeed it is important to understand then the magnetic behaviors and to establish the magnetic pathways (direct, indirect exchanges etc.).

This part of the study is also undertaken by the determination of the magnetic structures using the low temperature NPD data (RT and LT patterns are shown at the bottom of the page). In both cases, no structural transition *vs.* temperature is observed; magnetic peaks are well defined, of strong intensity and without broadening, i.e. characteristic of long range antiferromagnetism. Comparing these patterns where the magnetic peaks are highlighted by arrows, it is clear that the corresponding structures are different with magnetic propagation vectors: (0 0 ½) and (0 0 0) for x= 1 and 1.5, respectively, but also different from what is reported for Fe_3BO_5. A detailed description of these structures will be published rapidly, combined with the macroscopic magnetic properties and electrical measurements.

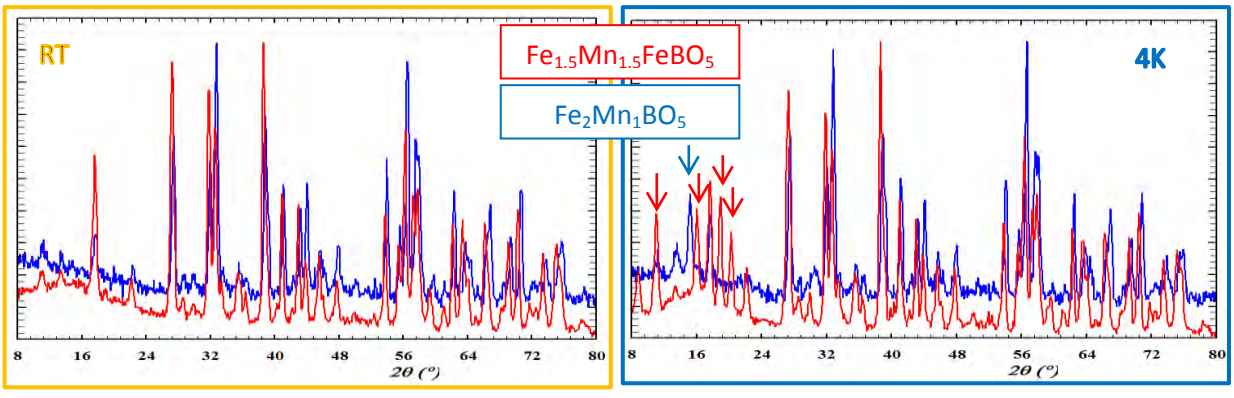

Neutron diffraction study of new oxyfluoride cathode materials for lithium batteries

Neutron Physics Laboratory - Neutron diffraction

Emad Maawad

Proposal ID

214

Experimental Report

Neutron diffraction study of new oxyfluoride cathode materials for lithium batteries

E. Maawad[1], R. Chen[2]

[1]Helmholtz-Zentrum Geesthacht, 21502 Geesthacht, Germany

[2]Karlsruhe Institute of Technology (KIT), Institute of Nanotechnology, 76344 Eggenstein-Leopoldshafen, Germany

Experimental results:

Recently, a new high-capacity (> 400 mAh g^{-1}) and high energy density (> 1000 Wh kg^{-1}) cathode material Li_2MO_2F (M = V, Cr) has been synthesized and developed at KIT (patent application: *EP 14160894.3*, 2014; S. Ren, R. Chen, E. Maawad, et al, *Adv. Sci. 2015*, accepted). The first Neutron diffraction experiments (**Fig. 1**) were successfully performed at FRM II (Garching, Germany) to study the crystal structure of such new compound. It has disordered cubic rock-salt symmetry, space group *Fm*-3*m*, *a* = 4.1 Å. In the present experiments performed at the MEREDIT beamline of the CANAM, the neutron diffraction patterns for three cycled Li_2MO_2F were recorded at 25°C with a wavelength of 1.4600 Å, with a mosaic Cu monochromator (**Fig. 2**). Due to the nanocrystalline character (about 10 nm) of the studied powder samples, the signal resolution is low relatively with a measure time of about 18h. Conversion of the diffraction peaks to *d*-spacings allows a comparison between the present patterns for the cycled samples and the previous one for the pristine material (Fig. 1). All main diffraction peaks such as (111), (200) and (311) can be still resolved from the present experiments. These results confirm that the crystal structure remains after cycling. Further refinement will be performed to extract the information such as cationic site occupancy. The obtained crystal structure information is essential for learning the lithium storage mechanisms, the structural stability and for subsequent optimization of material synthesis.

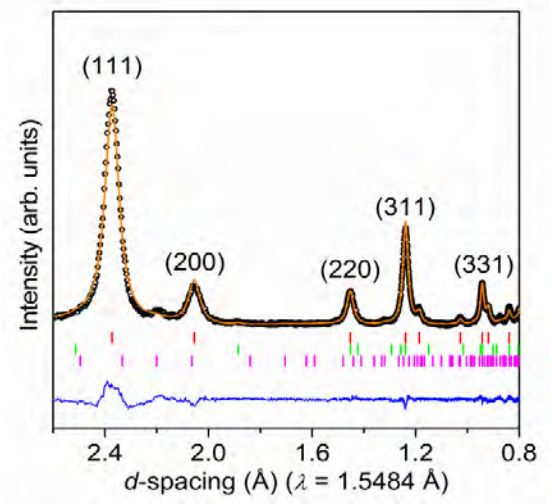

Fig.1: Previous neutron diffraction pattern (from FRM II) for the new compound Li_2MO_2F.

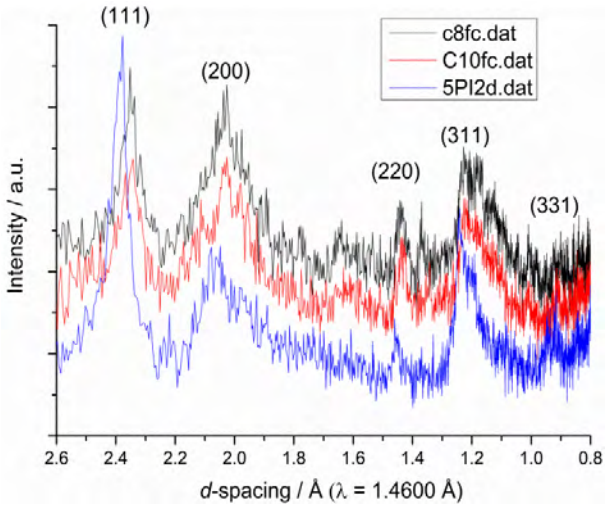

Fig. 2: Neutron diffraction patterns (at the CANAM) for three cycled Li_2MO_2F.

Activation of Lu-176 in newly designed ampoule

Neutron Physics Laboratory - Nuclear analytical methods with neutrons

Daniel Seifert

Proposal ID

211

New system for production of reactor medical radionuclides tested with enriched $^{176}Lu_2O_3$ target

D. Seifert, M. Kropáček, M. Tomeš, J. Kučera,
O. Lebeda; Nuclear Physics Institute of the CAS, v. v. i., Řež, Czech Republic

Development and testing of a new system for irradiation and subsequent processing of reactor targets

Materials and Methods

A new type of an irradiation vessel consisting of external aluminum alloy cover and inner quartz tube for sample placement was designed and tested. The system is water-proof. The ampoule was designed as disposable and was tested for He leak – the achieved leakage level was in order of 2×10–9 mbar.l/s under real irradiation conditions.

Results

Bombardment time: 70.45 hours, enriched $^{176}Lu_2O_3$
Neutron flux density: max. 10^{14} $cm^{-2}s^{-1}$ (LVR-15 reactor in ÚJV Řež, a. s.)
Processed: 7 days after EOB
Dissolving pattern: 10 min in 0.5 ml of 0.05M HCl at room temperature resulted in 65% activity recovery, the next identical dissolving step increased the recovery to 97.9 %.
Activity concentration: 21.8 GBq/ml in 0.05 M HCl

Conclusion

Experiments performed under the highest available neutron flux density have shown reproducible behaviour of the system regarding leakage, target processing and activity recovery.

The designed system demonstrated suitability for production of high-level activities of reactor medical radionuclides, in particular of ^{177}Lu.

Understanding Interactions in Colloidal Dispersions and the Effects of Multiple Scattering

Neutron Physics Laboratory - Neutron diffraction

Adrian Rennie

Proposal ID

179

Experiment

In this experiment, the effect of multiple scattering with polystyrene latex samples in D_2O/H_2O. The latex PS3 has been characterized using different techniques such as SEM, AFM, light scattering, zeta potential measurement, SAXS, SANS and etc. on various instruments [1,2,3]. Thickness and concentration of the sample are the two major factors that alter multiple scattering. PS3 samples were prepared in D_2O with 0.2, 0.5, 1 at low salt concentration (1×10^{-4} M NaCl) and a high concentration sample (8 wt%) with no salt. Each sample was filled into cells with 1 and 2 thickness allowing measurements at four concentrations and three thicknesses. The latex has the scattering length density of 1.41×10^{-6} Å^{-2} and D_2O 6.35×10^{-6} Å^{-2}. The data were collected on the double-crystal diffractometer MAUD and has been analysed using SASView and SASProFit [4].

Results and discussion

The data were fitted for all concentrations and thicknesses using both fitting programs. The results were up to 5% divergent regarding the size distribution and volume fractions. The difference could be attributed to the different models used in each program. SASView can take particles interactions into account, whereas in SASProfit all the scatterers are considered to be 'hard spheres' with no charge. On the other hand, multiple scattering effects have not been included in SASview, while SASProfit has modelled the multiple scattering that changes with thickness and concentration of the sample [4].

In order to investigate the effect of multiple scattering, data from different sample thicknesses and concentrations have been fitted with the same particle size, polydispersity and slit smear factor. At low concentrations (0.2, 0.5 and 1 wt%), a sphere model with no antiparticle structure factor S(Q) could adequately fit the data. The only fitting parameter changed between different data is the scaling factor for the intensity. At a higher concentration (8 wt%), interparticle interaction is taken into account for particles with 35 mV potential. The scattering pattern for 1 and 3mm thick samples at 0.5wt% concentrations are shown in Figure 1. The broadening of the scattering and divergence of the fit close to the minima (approximately 8×10^{-3} Å^{-1}) is more pronounced on increasing the thickness from 1 to 3 mm. Similar comparison was done the other concentrations and different thicknesses.

If the effect of multiple scattering is not significant, the plot of the ratio of the intensity for dilute samples having different thickness or different concentration should be constant and equal to a constant scaling factor apart from differences in interactions.

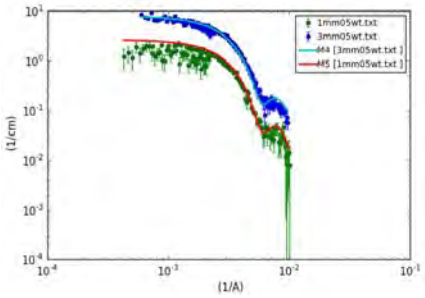

Figure 1. Scattering pattern and fits to the data for 1 mm and 3 mm 0.5 wt% latex in D_2O (no multiple scattering).

This comparison has been made for all the samples in the Q range around the intensity minima. The intensity for an individual pattern is divided by the scaling factor before plotting the ratios. Deviation of the ratios from 1 is an indication of the smearing caused by the multiple scattering. Figure 2 is an example of intensity ratios, for the samples in different thicknesses. Generally larger deviations were observed for the thicker and higher concentration samples. The effect is easier to observe for the 8 wt% data but it is within the error bar in the lower concentration.

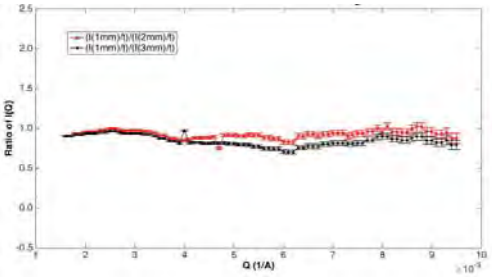

Figure 2. The intensity ratio between 1 mm and 3 mm thicknesses of 8 wt% PS3/D_2O sample.

Conclusions

The broadening of the peak and changes in the intensity ratio caused by multiple scattering, were compared between different concentration and thicknesses. The concentration and the thickness of the sample give rise to the multiple scattering. The effect is significant for the 8% data and is of the same order as the effects of interparticle interactions but occurs in different regions of Q. Further modelling to include treatment of multiple scattering with appropriate interactions is in progress.

[1] A. R. Rennie at al. J. Appl. Cryst., 2013, 46(5): 1289-1297.
[2] M. S. Hellsing, et al. RSC Advances, 2012, 2, 7091– 7098.
[3] M. S. Hellsing et al. Appl. Phys. Lett. 2012, 100, 221601.
[4] J. Saroun, J. Appl. Cryst. 2000, 33, 824-828.

Radiation Hardness of Si Pixel Chips and Components for ALICE Inner Tracker System Upgrade Project

Laboratory of Cyclotron and Fast Neutron Generators

Jozef Ferencei

Proposal ID

60

CANAM project:
"Radiation Hardness of Si Pixel Chips and Components for ALICE Inner Tracker System Upgrade

During the course of 2013 year the following measurements were made in U-120M cyclotron of Nuclear Physics Institute in the framework of CANAM project Nr. 60 "Radiation Hardness of Si Pixel Chips and Components for ALICE Inner Tracker System Upgrade":

1. Series of measurements to determine Single Event Upset (SEU) probability for SRAM memories in 180 nm technology from TowerJazz foundry in Israel, foreseen for mass production of silicon pixel chips for ALICE inner tracker system upgrade. Results confirmed the acceptable SEU rate at the level of 10^{-13} cm^2bit^{-1} causing rather tolerable data corruption (~10^{-9} bit^{-1} for central most affected chip) with no necessity for special expensive protections. This is important verification of technology suitability for production of monolithic active pixel sensors (MAPS) with on-chip integrated electronics. Measurements at U-120M cyclotron together with the ones carried at higher energies in Paul Scherer Institute in Villigen, Switzerland are part of the published "*Technical Design Report for the Upgrade of the ALICE Tracking System*", CERN-LHCC-2013-024, ALICE-TDR-017, which is available at CERN document server using the following URL: http://cds.cern.ch/record/1625842/files/ALICE-TDR-017.pdf?version=3 (pages 38-39). This document was submitted to 116th meeting of LHC Experiments Committee held on 4.12.2013 for endorsement. Investigations will continue using higher beam currents to study Single Event Latch-ups, i.e. the functional failure studies.
2. After careful selection procedure made in CERN the suitable fast (up to 6 Gbit/s) signal cable candidate 30 AWG Micro Twinax Cable from Samtec Company was chosen. Proton irradiation up to the total ionization dose of 1 Mrad was made in U-120 M cyclotron. The cable was shipped back to CERN, where measurements using fast oscilloscope with specialized pseudo random bit sequence generator confirmed unchanged bit error rate probability. This activity will continue for the laminated version of same type of cable, which is more compact w.r.t. non-laminated version.
3. For ALICE Inner Tracker System upgrade project the field-programmable gate arrays (FPGA) are foreseen to cope with expected enormous data volume (up to 30 Gbit/sec). As these FPGA will be located in LHC accelerator radiation environment, the unavoidable selection procedure of radiation hard commercially available FPGA was initiated. To precede with this complex task two PhD students from Faculty of information technology Czech technical university in Prague joined our group. First test measurements using Xilinx Spartan XC3S200 FPGA were already made. The detailed radiation hardness studies of modern Flash FPGA (expected to be more radiation hard) SmartFusion2 from Microsemi Company are in preparation.